Mean-field theory of the DNLS equation at positive and negative absolute temperatures

Michele Giusfredia,b,c, Stefano Iubinib,c, Antonio Politid,b, Paolo Politib,c,*

^aDipartimento di Fisica e Astronomia, Università di Firenze, via G. Sansone 1 I-50019, Sesto Fiorentino, Italy
 ^bIstituto dei Sistemi Complessi, Consiglio Nazionale delle Ricerche, via Madonna del Piano 10, I-50019 Sesto Fiorentino, Italy
 ^cIstituto Nazionale di Fisica Nucleare, Sezione di Firenze, via G. Sansone 1 I-50019, Sesto Fiorentino, Italy
 ^dInstitute for Complex Systems and Mathematical Biology University of Aberdeen, Aberdeen AB24 3UE, United Kingdom

Abstract

The Discrete Non Linear Schrödinger (DNLS) model, due to the existence of two conserved quantities, displays an equilibrium transition between a homogeneous phase at positive absolute temperature and a localized phase at negative absolute temperature. Here, we provide a mean-field theory of DNLS and show that this approximation is semi-quantitatively correct in the whole phase diagram, becoming exact in proximity of the transition. Our mean-field theory shows that the passage from stable positive-temperature to metastable negative-temperature states is smooth.

Keywords: Negative temperature, mean-field theory, phase transitions

1. Introduction

The Discrete Non Linear Schrödinger (DNLS) equation is around fifty years old, but it continues to attract the interest of researchers [1, 2, 3] for at least two reasons. On the one hand, it has applications in a variety of different fields, ranging from the foundations of statistical mechanics [4] to solid-state physics [5]. On the other hand, its nonlinear and non integrable character is the basis of interesting non-trivial properties: from a dynamical point of view, the existence of localized breathers [6], and from a statistical point of view, the presence of a negative-temperature (T) regime [7] in a large part of its phase diagram. The two properties are strictly related, because the negative–T phase is characterized by the spontaneous emergence of breathers, which are in principle metastable [8] (the "equilibrium" state corresponds to a single breather sitting on top of an infinite-temperature background [9]). However, because of the extremely slow breather dynamics [10] (due to the spontaneous appearance of an adiabatic invariant [11]), the asymptotic state may be effectively unachievable [9].

Email addresses: michele.giusfredi@unifi.it (Michele Giusfredi), stefano.iubini@cnr.it (Stefano Iubini), a.politi@abdn.ac.uk (Antonio Politi), paolo.politi@cnr.it (Paolo Politi)

According to Machlup's criterion, the existence of a negative—T phase is a general property of statistical systems displaying a finite energy density at infinite temperature [12]. In the DNLS case, this occurs because of the existence of two conserved quantities bounded from below: the energy and the mass (or norm). The purely stochastic C2C model [7, 13, 14] (where the energy is locally the square of the mass) is an even simpler example and represents a very good training ground, since the absence of interactions between neighbouring sites makes it possible to derive some rigorous results [15, 16]. Furthermore, it helped establishing a connection with a wider class of stochastic models [17, 18], the so called Zero Range Processes [19].

In this paper we introduce a mean-field (MF) description of the DNLS. The approximation is based on a tweak of the interaction term: we replace the product of variables $x_n x_{n+1}$ on neighbouring sites, with the product between the variable on a given site with its statistical average along the system, $x_n \langle x_n \rangle$. As a result, the grand-canonical partition function can be factorized, thereby obtaining explicit formulas and reaching a better comprehension of some properties of the DNLS model. The MF approximation is exact in proximity of the transition line separating the homogeneous (T > 0) phase from the localized (T < 0) one. The reason is that spatial correlations are absent and the average contribution of the interaction energy vanishes along such a curve. In addi-

^{*}Corresponding author

tion, the MF approximation gives a consistent and semiquantitatively correct description in the whole phase diagram, including the T=0 curve and the (metastable) negative T region. In Sec. 2 we present the model and the method. The main results of the MF approximation are discussed making a distinction between positive (Sec. 3) and negative (Sec. 4) temperatures, because in the latter case it is necessary to introduce a cutoff in the mass integral which defines the partition function. All the details of the calculation and of the simulations are deferred to the appendices.

2. The Model and its Mean Field Theory

We start by defining the DNLS model and recalling the most important properties of its phase diagram. As usual, we consider a one dimensional lattice of size Nand associate a local mass c_n and a phase ϕ_n to each site n. The system Hamiltonian is

$$H = \sum_{n} \left[c_n^2 + 2J \sqrt{c_n c_{n+1}} \cos(\phi_n - \phi_{n+1}) \right] \equiv Nh \quad (1)$$

where h is the energy density and $J \ge 0$ modulates the hopping energy.¹ The dynamical equations are $\dot{c}_n = -\partial H/\partial \phi_n$ and $\dot{\phi}_n = \partial H/\partial c_n$. The mass

$$A = \sum_{n} c_n \equiv Na, \tag{2}$$

as well as the energy, is conserved.

The ground state is characterized by uniform masses $(c_n = a)$ and alternating phases $(\phi_{n+1} = \phi_n + \pi)$. The ground state energy is therefore

$$h_{GS} \equiv \frac{H}{N} = a^2 - 2Ja. \tag{3}$$

The transition line between positive and negative temperatures is characterized by an exponential distribution of masses and a random distribution of phases, which implies

$$h_c = 2a^2. (4)$$

The negative—T region appears above the critical line and its properties are not yet fully understood [14, 17, 20]: they depend on the size of the system, on the statistical ensemble describing it, and on the time scales over which we observe the system, because the homogeneous phase is actually metastable above the critical line.

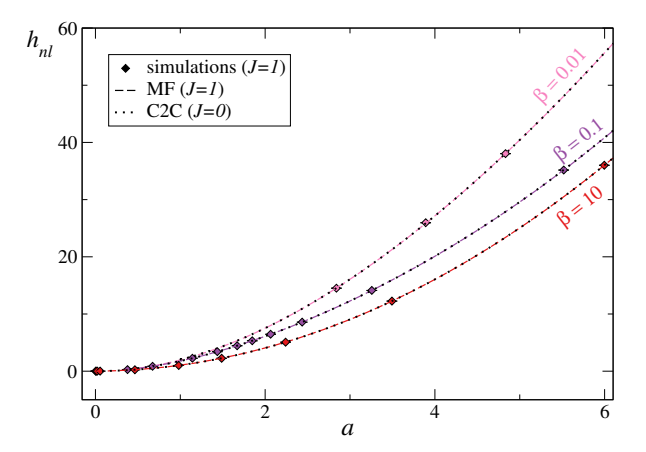


Fig. 1: Value of h_{nl} along three isothermal curves ($\beta = 0.01, 0.1, 10$ from top to bottom) comparing the results of equilibrium numerical simulations (see Appendix A) of the DNLS equation (symbols) with the prediction of the MF theory (dashed lines) and with the energy of the C2C model (dotted lines) as derived in [21, 22].

As from Eq. (1), the energy density is the sum of two contributions: the local energy, $h_{nl} = \langle c_n^2 \rangle$, and the interaction energy, $h_{int} = \langle 2J \sqrt{c_n c_{n+1}} \cos(\phi_n - \phi_{n+1}) \rangle$. In order to better appreciate the amplitude of the two contributions, it is instructive to compare the DNLS (1) with the limit case J = 0, when the energy density is composed of the h_{nl} term only, the angular variables being absent therein. Actually, J = 0 corresponds to the so-called C2C model, where the evolution is determined by a local stochastic dynamical rule that ensures conservation of both mass and energy [13].

In Fig. 1, we plot the numerical values of h_{nl} for the DNLS for different temperatures as a function of the mass density a and for J=1. Interestingly, they align almost perfectly along the corresponding isothermal lines of the C2C (J=0), showing that given the mass density and the temperature, the nonlinear energy h_{nl} (approximately) coincides in the two models. This implies that the angular degrees of freedom contribute "simply" as an additional interaction energy h_{int} , bounded between -2aJ in the ground state and 0 on the critical line.

Within the grand canonical formalism, the equilibrium properties of DNLSE can be extracted from the partition function

$$Z(\beta,\mu) = \int_0^\infty \prod_n dc_n \int_0^{2\pi} \prod_n d\phi_n e^{-\beta(H+\mu A)}, \quad (5)$$

where β is the inverse temperature, μ is the chemical potential, while the energy H and the mass A are given by Eqs. (1-2). The function was evaluated in Ref. [23], determining the leading eigenfunction of a suitable trans-

¹Negative values of *J* can be mapped to positive ones via the gauge transformation $\phi_n \to \phi_n + \pi n$ [1].

fer integral operator. However, the final expressions are not very handy for the extraction of useful information. Altogether, the main obstacle is that for J > 0, the interaction energy prevents a factorization of the integrals. Here, we show that a suitable mean field approximation restores the factorization while still providing and accurate description of the equilibrium regime in a large portion of the parameter space and, in particular, in the high-temperature region.

The approximation consists in rewriting the product of masses appearing in the neighbouring-site coupling term, as

$$\sqrt{c_n c_{n+1}} \simeq q \sqrt{c_n},\tag{6}$$

where $q \equiv \langle \sqrt{c_n} \rangle$ is a statistical average to be determined autoconsistently with Z. Within this approximation, the Hamiltonian H is rewritten as

$$H_{MF} = \sum_{n} \left[c_n^2 + 2qJ \sqrt{c_n} \cos(\phi_n - \phi_{n+1}) \right]$$
 (7)

and the partition function becomes the product of single-site terms, $Z_{MF} = z^N$, with

$$z(\beta,\mu) = \int_0^\infty dc \int_0^{2\pi} d\varphi e^{-\beta(c^2 + 2qJ\sqrt{c}\cos\varphi) + mc}, \qquad (8)$$

where φ is the phase difference between neighbouring sites, and $m \equiv \beta \mu$.

The integral over the angle φ can be easily calculated, introducing the zero-order modified Bessel function,

$$z(\beta,\mu) = 2\pi \int_0^\infty dc \, \exp\left(-\beta c^2 + mc\right) I_0(2\beta q J \sqrt{c}), \quad (9)$$

where q, as anticipated, must be determined autoconsistently through the relation

$$q \equiv \langle \sqrt{c} \rangle = \frac{2\pi}{z} \int_0^\infty dc \ \sqrt{c} \exp\left(-\beta c^2 + mc\right) I_0(2\beta q J \sqrt{c}). \tag{10}$$

Similar expressions can be also derived for the mass density $a = \langle c \rangle$ and the energy densities $h_{nl} = \langle c^2 \rangle$ and $h_{int} = \langle 2qJ\sqrt{c}\cos\varphi\rangle$. Without loss of generality, from now on we will assume J=1, because J can be scaled out so long as it is strictly larger than 0.

If $\beta > 0$ the convergence of the integrals appearing in the definition of the various observable is ensured, while for $\beta < 0$ the integrand diverges at large c, signaling the well known instability due to the appearance of large peaks (breathers). For this reason, negative temperatures require a special treatment and we have thereby devoted an entire section to their discussion. In a few words, while negative-temperature localized states in the DNLS model are formally well-defined

only in the microcanonical ensemble [17, 18, 3], homogeneous, metastable states have been recently shown to admit a consistent description in terms of a regularized grand canonical theory [20]. In this paper we will restrict ourselves to this class of negative-temperature states.

A first direct confirmation of the validity of the mean field approximation is offered in Fig. 1 where we see that the MF estimates of h_{nl} reproduce very well the numerical observations.

Independently of the sign of β , it is convenient to introduce the smallness parameter $w=1/(\beta\mu^2)=\beta/m^2$ ($m=\beta\mu\to-1/a$ for $\beta\to0$), which allows deriving simple and accurate formulas in the small $|\beta|$ region (see Appendix B for the derivation of the expressions for the most relevant observables).

For instance, at leading order in w, the following expressions hold across the critical line, i.e., for both positive an negative temperatures:

$$q = \frac{\sqrt{\pi}}{2\sqrt{|m|}} - \frac{7\sqrt{\pi w}}{8\sqrt{|m|}} + O\left(w^2\right) \tag{11}$$

$$a = \frac{1}{|m|} - \frac{4w}{|m|} + O\left(w^2\right) \tag{12}$$

$$h_{nl} = \frac{2}{m^2} - \frac{20w}{m^2} + O\left(w^2\right) \tag{13}$$

$$h_{int} = -\frac{\pi}{2}w + O\left(w^2\right). \tag{14}$$

In Fig. 2 we report the relative error on the MF-value of the single-particle partition function $z(\beta, \mu)$ versus the approximation order k, for some values of w (both for positive and negative temperatures). As expected, the very high accuracy for small w values degrades when w becomes of order 1. A second feature is that the accuracy of the expansion initially increases with k up to some k^* , when it starts degrading. This is a clear indication of the asymptotic nature of the series expansion in powers of w. Finally, the overlap of data obtained for the same w but different β values indicate that w is indeed the only relevant parameter controlling the accuracy of the expansion.

3. Positive temperatures

In the positive–T regime, the equilibrium state can be equivalently described by the microcanonical and

²The numerical results have been obtained by using Mathematica software, setting its parameters to ensure a sufficient precision of the calculations.

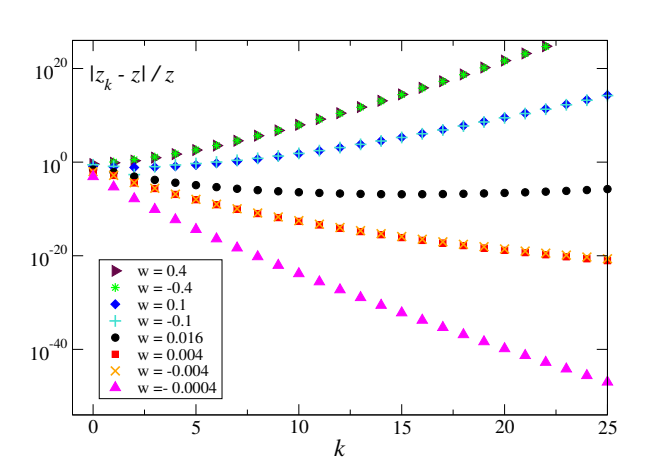


Fig. 2: Relative difference between the MF partition function z computed by numerically integrating the exact expression (9) and its analytical approximation z_k obtained as a series expansion at order k in w. The various symbols correspond to different w values as from the legend. The value of β is always equal to ± 0.4 except for the lowermost curve, where $\beta = -0.01$. Notice that the sign of β coincides with the sign of w. For negative β , the numerical integration is performed by imposing the same cutoff c^* as in the C2C model.

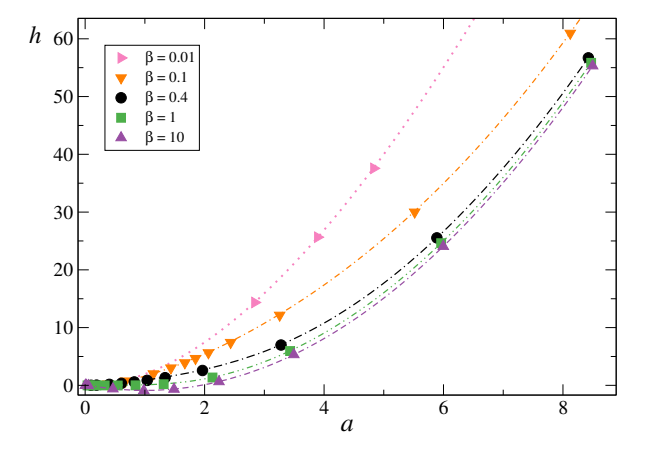


Fig. 3: Comparison between MF theory (curves) and exact results obtained via grandcanonical simulations (symbols). Each curve corresponds to a different $T=1/\beta$, increasing from bottom to top according to the legenda. The size of the system is N=100 and details about simulations are given in Appendix A.

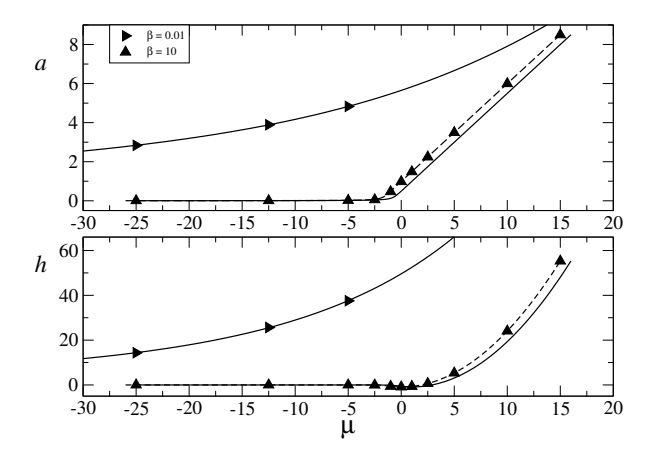


Fig. 4: Same as in Fig. 3, but we now compare MF and exact numerical results in the planes (μ, a) and (μ, h) rather than in (a, h). In this way a horizontal shift at low temperature is evident, due to a wrong determination of the chemical potential in the MF theory. Symbols: exact results from grandcanonical simulations. Full lines: MF approximation. Dashed lines: MF approximation corrected for the chemical potential: $\mu \rightarrow \mu - 1$.

the grandcanonical ensemble [17, 18]. Within the MF approximation, this means that the single-site partition function, see Eq. (8), is well defined and finite for any $\beta \ge 0$ and for any m (i.e., for any μ).

In Fig. 3 we plot various MF isothermal curves in the plane (a, h), with $0.01 \le \beta \le 10$, and compare them with virtually exact points obtained via grandcanonical simulations performed for the same β values and different chemical potentials. These data show that the isothermal curves h(a) are very well reproduced by the MF theory. However, such curves do not tell the whole story.

In Fig. 4, the validity of the MF theory is tested in the planes (a, μ) and (h, μ) . There, we see that the agreement with the numerical data is very good at high T, while it worsen with decreasing T. Remarkably, it appears that the deviation essentially amounts to a shift of the chemical potential by one unit, as it can be appreciated by looking at the dashed curve, which corresponds to $\mu - 1$. As shown in Appendix C, the shift is a rigorous property at zero-temperature, and it is essentially irrelevant while approaching the transition line for finite a since μ diverges therein, so that the curves for μ and $\mu - 1$ practically coincide.

We now discuss the relative role of h_{nl} and h_{int} , an aspect of DNLS that has been little considered in its studies. From the literature, we know only that h_{int} vanishes on the critical line, which is the reason why C2C model is statistically equivalent to DNLS in its proximity. This is also the reason why the MF approximation

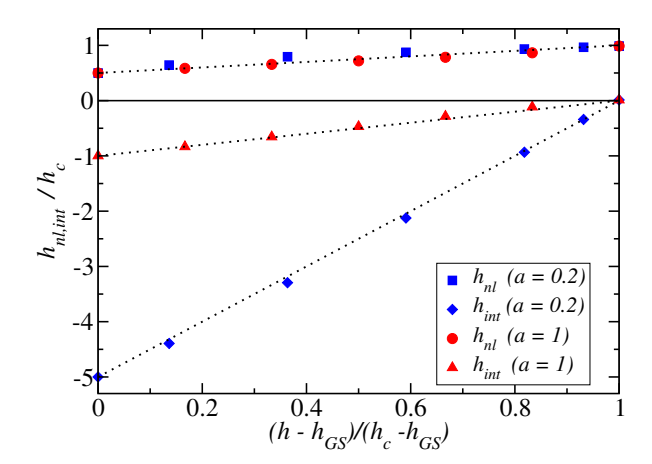


Fig. 5: The contributions h_{int} and h_{nl} are presented versus the total energy h suitably rescaled (see the main text). Symbols are the exact results from microcanonical simulations, as described in Appendix A, but with the removal of the interaction with the heat bath and starting from an initial condition with the chosen values of a and h.

is exact in such limit. Here below we try to understand more quantitatively how the energy distributes between the two terms, both in the exact DNLS theory and in its MF approximation.

In Fig. 5 we present the dependence of h_{nl} and h_{int} vs the total energy h, for two values of the mass density. In order to facilitate the comparison, the total energy is suitably shifted and scaled in such a way that the zero of the horizontal axis corresponds to T=0, while 1 corresponds to infinite temperature. This corresponds to plot $x=(h-h_{GS})/(h_c-h_{GS})$. Similarly, the two energy terms are scaled by the critical energy; so we plot $y_{nl,int}=h_{nl,int}/h_c$. Using the new variables, we have $y_{nl}(0)=\frac{1}{2}$ and $y_{nl}(1)=1$, while $y_{int}(0)=-1/a$ and $y_{int}(1)=0$.

It is quite surprising that both functions $y_{nl,int}(x)$ are very close to linear, with $y_{int}(x) \simeq (x-1)/a$ varying between -1/a and 0 and $y_{nl}(x) \simeq (x+1)/2$ varying between 1/2 and 1. The first result means that the contribution of the coupling term is vanishingly small for large a; the second result means that the contribution of the nonlinear term does not depend on a.

It is worth stressing that the same linear behaviors are expected in the MF approximation, because the limiting values of the two contributions, $y_{nl,int}(0, 1)$, are the same, see Appendix B and Appendix C, and because the exact and MF theories compare very well in the (a, h) plane, see Figs. 1,3. Nevertheless, it is not feasible to derive analytically the linear behavior of $y_{nl,int}(x)$ within the MF theory, because such theory works with the grand-canonical variables β , μ and their relation with a and b can be easily obtained numerically, but no closed-form

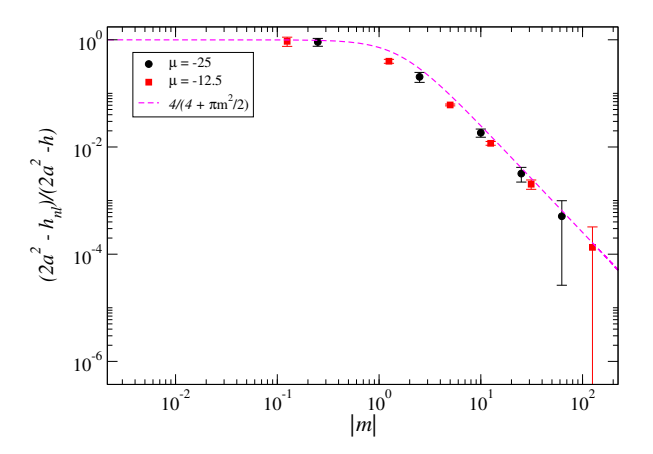


Fig. 6: This figure intends to represent the relationship between the total energy h of the system and its nonlinear part, h_{nl} . For small β both quantities tend to $h_c = 2a^2$, therefore we plot the relative differences between the two energies and the critical energy. The depedence of this ratio on m is well accounted for by the MF result (dashed line).

solutions are available. However, we can use the expansions in *w*, which is what we are going to do now.

For this purpose we have identified a quantity that for small w depends on a single parameter, namely m (see Appendix D),

$$R = \frac{h_c - h_{nl}}{h_c - h} \ . \tag{15}$$

This is the ratio between the distance of the nonlinear energy from the $\beta=0$ value (for the same mass density) and the distance of the full energy, again from the $\beta=0$ value.

In the positive-temperature region both terms of R are positive. Moreover, since $h_{int} \leq 0$, then the numerator is smaller than the denominator so that $0 \leq R \leq 1$. However, it is not straightforward to identify the locations in parameter space where the limit values can be achieved. In fact, for R being equal to 1, it is necessary that $h_{int} = 0$, which occurs when the denominator and the numerators are both equal to 0. Furthermore, R = 0 requires $h_{nl} = 2a^2$, which again occurs when the denominator vanishes.

MF analysis helps clarifying the issue, as shown in Fig. 6, where we plot R for different values of μ and β , comparing numerical results for the full DNLS model (symbols) with the analytical curve $R = 4/(4 + \pi m^2/2)$, found within the MF approximation, in a w-expansion. At the lowest order in w, R is only function of m, not of m. It is worth remembering that $m = \beta \mu$ is equal to -1/a on the critical curve $\beta = 0$. On the other hand, if we fix μ and vary β , the limit of small β corresponds to small m. Let us start from this limit, because for $\beta \to 0$, $h_{nl} \to 0$

and $R \to 1$: this is what we observe in Fig. 6. We can also monitor the regime $|m| \ll 1$, provided that w is small. On the critical curve, this simply implies $a \ll 1$ and in this limit $R \simeq a^2$, which means that for small mass density a, when h approaches h_c , h_{nl} is practically on the critical curve.

It is worth stressing that the approximation $R = 4/(4 + \pi m^2/2)$ is not valid for vanishing T. In this limit m diverges, which would imply a vanishing R, while in reality R goes to a constant,

$$\lim_{T \to 0} R = \frac{a^2}{a^2 + 2a}.$$
 (16)

4. Negative-temperature homogeneous states

States with energy density above the critical line $h_c(a)$ display negative temperatures and are expected to develop a thermodynamic instability, resulting in the condensation of a macroscopic peak [23]. The theoretical description of this mechanism requires a microcanonical formalism, while the grand canonical measure is formally ill-defined [17, 18]. Recently it was shown that homogeneous states slightly above the critical line (i.e. with $|\beta| \ll 1$) are metastable, in the sense that the characteristic time to develop the localization instability grows exponentially with |T| [20]. In this regime, an effective grand-canonical description can be developed in terms of an asymptotically unstable thermodynamic potential with a metastable region for low-amplitude states. The fundamental properties of the effective potential were derived in [20] under the approximation that the hopping term of the DNLS Hamiltonian is negligible with respect to the nonlinear one, thus removing any explicit phase dependence. In the following, we generalize this derivation including phases, within the MF approximation.

For β < 0, Eq. (8) is modified in order to introduce a cutoff c^* ,

$$z(\beta, m) = \int_0^{c^*} dc \, \int_0^{2\pi} d\phi \, \exp\left[-U(c, \phi; \beta, m)\right] \,, \quad (17)$$

where we have rewritten the exponent as a twodimensional potential having the form

$$U(c, \phi; \beta, m) = \beta c^2 + 2\beta q \sqrt{c} \cos \phi - mc.$$
 (18)

Notice that the parameters β and m are both negative. In Fig. 7 we plot the qualitative shape of potential (18) for $\phi = 0$ where the effect of the phase term is maximal, to highlight its effect. It contributes to destabilize the

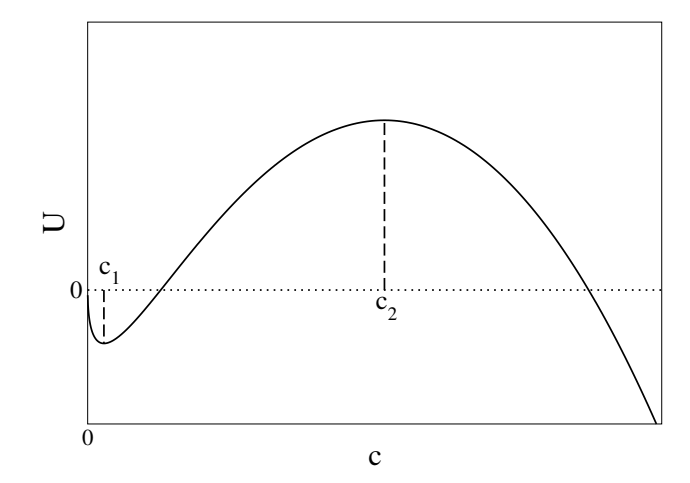


Fig. 7: Sketch of the potential U(c), Eq. (18), for $\theta=0$ and small, negative β .

c = 0 state which would otherwise be a minimum (as in the C2C model) for any $\beta < 0$.

The only confining term is the third one, due to the negative value of the chemical potential. Hence, in principle the potential is not necessarily confining at low c amplitudes. For a more quantiative analysis, it is convenient to distinguish among small, intermediate, and large c values: $U(c) \approx -\sqrt{c}, c, -c^2$, respectively.

The crossover from the first to the second regime occurs at $c_1 \simeq \beta^2 q^2/m^2$, while the crossover from the second to the third regime occurs at $c_2 \simeq |m/\beta|$. For the potential to be partially confining, it is therefore necessary that c_2 is sufficiently larger than c_1 . This implies $|m| \gg |\beta| q^{2/3}$, which, in the limit of small β , leads to $a \ll 1/|\beta|^{3/4}$ (see Eqs. (11,12) and a comment in the conclusions, next section). In this limit, $|U(c_1)| \ll U(c_2)$, so that the anisotropic term is fully negligible and the potential barrier matches the one derived in [20]. In this regime, one can set the cutoff mass equal to the potential maximum, $c^* = c_2$. However, we also see that for "large" a (and fixed β), the potential is not locally confining and one must expect breathers to arise much more rapidly. This is at variance with the C2C model, where there is always a minimum in 0.

In Fig. 8 we plot the resulting MF potential both for positive and negative β . In the former case the potential is everywhere confining along the c axis; in the latter case it is confining for small c. Interestingly, the anisotropic term, giving rise to the \sqrt{c} behavior at vanishing c is practically never visible.

In Figs. 9 and 10, we compare the MF prediction with the outcome of direct numerical simulations of the original DNLS equations, analogously to what done

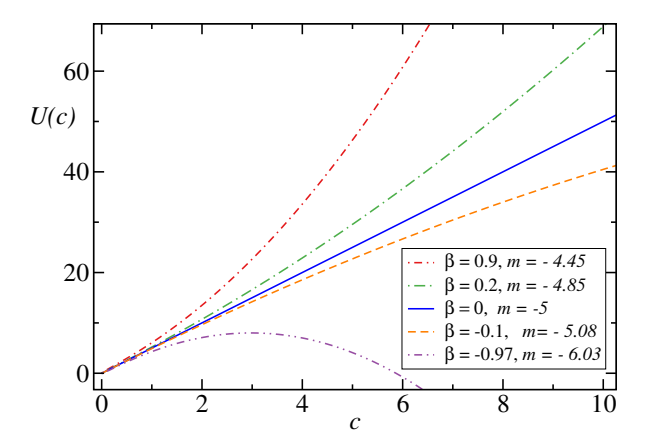


Fig. 8: MF potentials $U(c, \phi = 0) = \beta c^2 + 2q \sqrt{c} - mc$, for different values of β and m. The full (blue) line corresponds to $\beta = 0$ and U(c) is linear

in Figs. 3 and 4, but now for negative temperatures (see Appendix A).

5. Conclusions

In this paper, we have developed a mean-field approach to derive explicit expressions for the most relevant observables describing the equilibrium state of the DNLS equation. The approximation consists in assuming that the interaction is gauged by the average amplitude of the neighbouring sites rather than by their actual value.

In a certain sense, the mean-field approximation is a step forward compared to the stochastic C2C model in which the coupling term is completely neglected. In fact, the MF theory is accurate not only in the small β region, where the interaction energy is on average negligible: it turns out that the resulting approximation provide a good representation in a much wider region of the parameter space, including the correct determination of the T=0 curve,

It is also interesting to notice that the MF model provides an accurate description across the transition from positive to negative temperature, where instabilities are expected to arise. In fact, MF theories typically fail precisely in proximity of phase transitions. Here, the success of MF is due to the fact that the interaction energy is negligible in that area, and the transition itself occurs already in the absence interactions.

We stress two results: one concerns the negative—T region, the other regards the positive—T region. The former one is that above the critical curve the region of metastability seems to become increasingly narrow as the mass a increases, because metastability appears

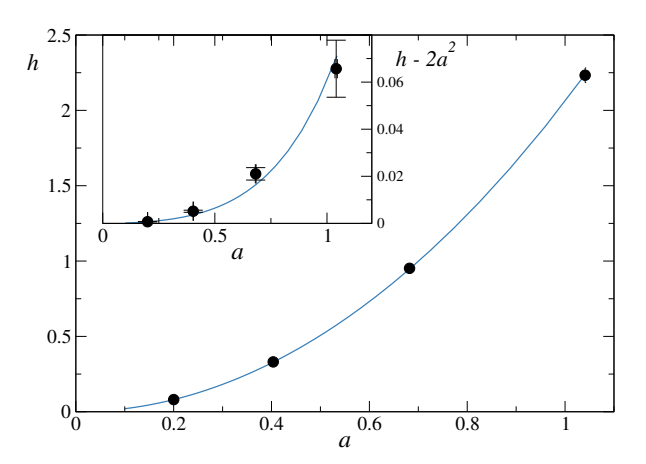


Fig. 9: Comparison of exact numerical results (circles) and MF prediction (blue line) for negative $\beta = -0.01$ and different values of m = -5, -2.5, -1.5, -1, from left to right. Main: comparison in the plane (a, h). Inset: comparison in the plane $(a, h - 2a^2)$. Here it is manifest we are in the negative-T region, because $(h - 2a^2) > 0$. We also make evident the statistical error bar for the circles, obtained as spatial and temporal averages of grandcanonical simulations.

for $|\beta| < a^{-4/3}$. However, passing to the (a, h) plane, this means that $h - h_c < (\pi/2 + 20a^2)a^{2/3}$, which is an increasing function of a.

The latter result is that the two energy terms, h_{nl} and h_{int} , display a rather remarkable linear dependence on the energy itself: a result valid well beyond the MF approximation.

We conclude the paper by asking whether it would be possible to extend this mean-field approach to provide an approximate description of the dynamical, nonequilibrium properties of the DNLS.

Data availability

Reasonable requests for data will be fulfilled.

Declaration of competing interest

The authors declare that they have no known competing financial interests or personal relationships that could have appeared to influence the work reported in this paper.

CRediT authorship contribution statement

MG did most of numerical simulations and calculations. All authors have contributed equally to the planning, discussions, and writing.

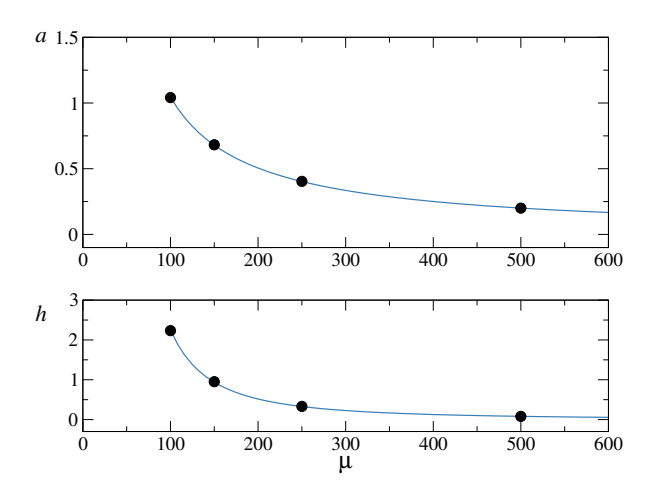


Fig. 10: As in Fig. 9, but now the comparison is done in the planes (μ, a) and (μ, h) rather than in the plane (a, h).

Declaration of generative AI and AI-assisted technologies in the writing process

Authors have not used generative AI and AI-assisted technologies in the writing process.

Acknowledgements

SI and PP acknowledge financial support from the Italian MUR PRIN2022 project "Breakdown of ergodicity in classical and quantum many-body systems" (BECQuMB) Grant No. 20222BHC9Z.

Appendix A. Technical details for numerical simulations

Simulations of the full DNLS model are performed on a chain of size N=100 with periodic boundary conditions interacting with a thermal reservoir on site n=1. The evolution is studied introducing the conjugate canonical variables

$$v_n = \sqrt{2c_n}\cos\phi_n, \ u_n = \sqrt{2c_n}\sin\phi_n, \quad n = 1,\dots, N,$$
(A.1)

whose time dependence is ruled by the following equations of motion

$$\dot{v}_n = -(v_n^2 + u_n^2)u_n - u_{n-1} - u_{n+1} \tag{A.2}$$

$$\dot{u}_n = (v_n^2 + u_n^2)v_n + v_{n-1} + v_{n+1}. \tag{A.3}$$

We have implemented this Hamiltonian dynamics by using a 4-th order Runge Kutta algorithm with an integration step $\delta t = 10^{-3}$.

The DNLS chain is thermostatted at temperature $T = \beta^{-1}$ and chemical potential μ with a Monte Carlo heat bath [24]. Once every t = 1 units of time, we generate new canonical variables for site 1, $u_1' = u_1 + \delta u_1'$ and $v_1' = v_1 + \delta v_1$, where δu_1 and δv_1 are random variables extracted from the uniform distribution in the interval [-0.5, 0.5]. Then, we update the canonical variables using a Metropolis algorithm by evaluating the cost function $W = \exp(-\beta \Delta E + m \Delta A)$, where

$$\Delta A = \frac{u_1'^2 + v_1'^2}{2} - \frac{u_1^2 + v_1^2}{2} = c_1' - c_1 \tag{A.4}$$

$$\Delta E = c_1'^2 - c_1^2 + (u_N + u_2)\delta u_1 + (v_N + v_2)\delta v_1$$
 (A.5)

are the variations in mass and energy respectively. When W > 1, we update u_1 and v_1 with u'_1 and v'_1 , while if W < 1 the move is accepted with probability W. This algorithm is implemented in the same way regardless of the sign of β [4].

Initial condition are typically selected as "infinite temperature" configurations, i.e. with phases ϕ_n extracted from the uniform distribution in $[0, 2\pi]$ and masses c_n generated from an exponential distribution $f(c) = 1/a_i \exp(-c/a_i)$, with the a_i chosen appropriately for each simulation so as to be close to the mass density reached at equilibrium.

The values of a, h and h_{nl} are obtained from a combination of spatial and temporal averages of local quantities. With the canonical variables u_n and v_n , the local masses are $c_n = \frac{1}{2}(u_n^2 + v_n^2)$. We can also define local energies ϵ_n as

$$\epsilon_n \equiv \frac{1}{4}(u_n^2 + v_n^2)^2 + \frac{1}{2}(u_{n-1} + u_{n+1})u_n + \frac{1}{2}(v_{n-1} + v_{n+1})v_n,$$
(A.6)

which correspond to the sum of the nonlinear local energy c_n^2 and half the coupling energy between sites n-1 and n and between n and n+1, so that $\sum_{n=1}^N \epsilon_n = H$. We first consider for each site a time average of c_n , ϵ_n and c_n^2 , with which we make spatial averages to get a, b and b are spectively. Time averages were made over times between b and b and b are units, after waiting for a transient b and b and b are units, after waiting for a transient b and b are special averages (to remove any effects due to the heat bath, connected to site b, the first and last b and b are special averages are obtained from the standard deviation of the spatial average and in all figures such uncertainties are either shown or they smaller than the symbol size.

Appendix B. Small- β expansion

In this appendix we derive the analytical expressions of the MF theory for small β .

Let us start with the case $\beta > 0$. The reduced grand canonical partition function of the MF model, Eq. (9) (J = 1),

$$z = 2\pi \int_0^\infty dc \, e^{-\beta c^2 + mc} I_0(2\beta q \, \sqrt{c})$$
 (B.1)

can be rewritten as

$$z = \int_0^\infty dc \sum_{n=0}^\infty e^{(-\beta c^2 + mc)} \frac{2\pi}{(n!)^2} (\beta q)^{2n} c^n,$$
 (B.2)

by using the Taylor expansion of the modified Bessel function I_0 ,

$$I_0(v) = \sum_{n=0}^{\infty} \frac{1}{(n!)^2} \left(\frac{v}{2}\right)^{2n}.$$
 (B.3)

Since the series in the integrand of (B.2) absolutely converges for any positive c, we can swap the order of integration and summation, then individually integrate the terms of the series, from which we obtain

$$z = \sum_{n=0}^{\infty} 2^{-n} \beta^{-(1+3n)/2} q^{2n} \pi U\left(\frac{1+n}{2}, \frac{1}{2}, \frac{m^2}{4\beta}\right), \quad (B.4)$$

where U is the Tricomi confluent hypergeometric function

Similarly, it is possible to obtain the average value of any power α of c as a function of β , m and q,

$$\langle c^{\alpha} \rangle = \frac{1}{z} \int_{0}^{\infty} dc \int_{0}^{2\pi} d\varphi \, c^{\alpha} \, e^{-\beta c^{2} + mc - 2\beta q \sqrt{c} \cos \varphi}$$

$$= \frac{2\pi}{z} \int_{0}^{\infty} dc \, c^{\alpha} \, e^{-\beta c^{2} + mc} I_{0}(2\beta q \, \sqrt{c})$$

$$= \frac{1}{z} \sum_{n=0}^{\infty} 2^{-n-\alpha} \pi \beta^{(n-1-\alpha)} (\beta q)^{2n} \Gamma(n+1+\alpha)$$

$$\times U\left(\frac{n+1+\alpha}{2}, \frac{1}{2}, \frac{m^{2}}{4\beta}\right),$$
(B.5)

from which we have the expression for the mass density a for $\alpha = 1$ and for the nonlinear energy h_{nl} for $\alpha = 2$. We can also express the self-consistency relation $q = \langle \sqrt{c} \rangle$ using Eq.(B.5) with $\alpha = 1/2$,

$$q = \langle \sqrt{c} \rangle = \frac{\pi}{z} \sum_{n=0}^{\infty} 2^{-n-1/2} \beta^{3n/2-3/4} \frac{q^{2n}}{(n!)^2} \Gamma\left(\frac{3}{2} + n\right) \times U\left(\frac{3}{4} + \frac{n}{2}, \frac{1}{2}, \frac{m^2}{4\beta}\right).$$
(B.6)

For the interaction energy density h_{int} we have instead

$$h_{int} = \frac{1}{z} \int_{0}^{\infty} dc \int_{0}^{2\pi} d\varphi \ 2q \sqrt{c} \cos \varphi e^{-\beta c^{2} + mc - 2\beta q \sqrt{c} \cos \varphi}$$

$$= -\frac{4\pi q}{z} \int_{0}^{\infty} dc \ \sqrt{c} e^{-\beta c^{2} + mc} I_{1}(2\beta q \sqrt{c})$$

$$= \frac{1}{z} \sum_{n=1}^{\infty} \frac{2^{-n} \beta^{-2 + 3n/2} m q^{2n}}{(n-1)!} U\left(1 + \frac{n}{2}, \frac{3}{2}, \frac{m^{2}}{4\beta}\right),$$
(B.7)

where we have used the expansion of I_1 ,

$$I_1(v) = \frac{d}{dv}I_0(v) = \sum_{n=1}^{\infty} \frac{n}{(n!)^2} \left(\frac{v}{2}\right)^{2n-1}.$$
 (B.8)

It is now convenient to introduce the smallness parameter $w = \beta/m^2$, which appears as the argument of the hypergeometric function U. In particular, $U(\cdot, \cdot, 1/4w)$ admits an asymptotic expansion for $w \to 0$ in terms of the generalized hypergeometric series ${}_2F_0$ [25],

$$U\left(a, b, \frac{1}{4w}\right) \simeq (4w)^a \, {}_2F_0(a, a - b + 1; ; -4w), \quad (B.9)$$

where ${}_{2}F_{0}(a, a-b+1; ; -4w)$ does not converge in w = 0 but exists as a formal power series in w.

From now on we will also consider m < 0. By replacing $\beta = wm^2$ and expanding U in powers of w in Eq. (B.4), we get

$$z = \frac{2\pi}{|m|} - \frac{4\pi w}{|m|} + \left(\frac{24\pi}{|m|} + 2m^2\pi q^2\right)w^2 + O(w^3), \text{ (B.10)}$$

that we can substitute in Eq. (B.6) to obtain

$$q = \frac{\sqrt{\pi}}{2\sqrt{|m|}} - \frac{7\sqrt{\pi}}{8\sqrt{|m|}}w + \frac{\sqrt{\pi}(449 + 16|m|^3q^2)}{64\sqrt{|m|}}w^2 + O(w^3, q^4).$$
(B.11)

The self-consistency relation can therefore be solved in a perturbative way at an arbitrary order of w, from which we obtain

$$q = \frac{\sqrt{\pi}}{2\sqrt{|m|}} - \frac{7\sqrt{\pi}}{8\sqrt{|m|}}w + \frac{449\sqrt{\pi} + 16|m|^2\pi^{3/2}}{64\sqrt{|m|}}w^2 + O(w^3).$$
(B.12)

Once we have q, we can replace it into the expressions (B.10), (B.5) and (B.7) to get

$$z = \frac{2\pi}{|m|} - \frac{4\pi}{|m|}w + \frac{\pi(24 + 2|m|^3q^2)}{|m|}w^2 + O(w^3) \quad (B.13)$$

$$a = \frac{1}{|m|} - \frac{4w}{|m|} + \left(\frac{40}{|m|} + \frac{|m|\pi}{4}\right)w^2 + O\left(w^3\right)$$
 (B.14)

$$h_{nl} = \frac{2}{m^2} - \frac{20w}{m^2} + \frac{\left(296 + m^2\pi\right)w^2}{m^2} + O\left(w^3\right) \quad (B.15)$$

$$h_{int} = -\frac{\pi w}{2} + \frac{15\pi w^2}{4} + O\left(w^3\right)$$
 (B.16)

$$h = \frac{2}{m^2} - \left(\frac{\pi}{2} + \frac{20}{m^2}\right)w + \left(\frac{19\pi}{4} + \frac{296}{m^2}\right)w^2 + O\left(w^3\right)$$
(B.17)

The combination of Eqs. (B.14) and (B.17) gives, for $T = \infty$ (i.e., for w = 0),

$$h = 2a^2$$
. (B.18)

Let us now consider the case where $\beta < 0$ and m < 0. We can write the reduced partition function z as

$$z = 2\pi \int_0^{\frac{m}{2\beta}} dc \, e^{-\beta c^2 + mc} I_0(2\beta q \, \sqrt{c}), \tag{B.19}$$

where the cutoff in the mass integration $c^* = \frac{m}{2\beta}$ is the same as that assumed in the study of the C2C model.

If we express β as $\beta = wm^2$ and expand the integrand function in powers of w up to order w^2 , we obtain

$$z \simeq 2\pi \int_0^{\frac{m}{2\beta}} dc \, e^{mc} \left(1 - c^2 m^2 w + c m^4 \left(\frac{c^3}{2} + q^2 \right) w^2 \right)$$
$$z = \frac{2\pi}{|m|} - \frac{4\pi}{|m|} w + \frac{\pi (24 + 2|m|^3 q^2)}{|m|} w^2 + O(w^3),$$
(B.20)

which is equal to Eq. (B.10). We therefore find that the expansion of z at negative temperatures coincides with that at $\beta > 0$. An adjustment of the cutoff leads only to corrections of order $e^{-1/(2|w|)}$.

Similarly, from the calculation of q, a, h_{nl} and h_{int} we find that the expressions (B.12-B.17) are also valid for $\beta < 0$.

Appendix C. T = 0 limit

In the low-temperature limit, we can approximate the expressions for the partition function z, a, q and h by using the leading term of the modified Bessel functions $I_{0,1}$ for large argument v

$$I_{0,1}(v) \simeq \frac{e^v}{\sqrt{2\pi v}}.$$
 (C.1)

By substituting (C.1) in Eq. (9), z can be rewritten as

$$z \simeq \int_0^\infty dc \, \sqrt{\pi} \frac{e^{\beta A(c)}}{\sqrt{\beta a}c^{1/4}},\tag{C.2}$$

where

$$A(c) = -c^2 + \mu c + 2q\sqrt{c}.$$
 (C.3)

We can now use the saddle-point method to approximate z as

$$z \simeq \sqrt{\pi} \frac{e^{\beta A(c^*)}}{\sqrt{\beta q} c^{*1/4}},$$
 (C.4)

where c^* is the mass value that maximizes A(c) and therefore satisfies the relation

$$\left. \frac{\partial A(c)}{\partial c} \right|_{c=c^*} = 2c^* - \frac{q}{\sqrt{c^*}} - \mu = 0. \tag{C.5}$$

We can also derive the expression for q in the low-temperature limit,

$$q \simeq \frac{1}{z} \int_0^\infty dc \, \sqrt{c} \, \sqrt{\pi} \frac{{\rm e}^{\beta A(c)}}{\sqrt{\beta q} c^{1/4}} \simeq \sqrt{c^*} \frac{\sqrt{\pi}}{z} \frac{{\rm e}^{\beta A(c^*)}}{\sqrt{\beta q} c^{*1/4}} = \sqrt{c^*},$$
(C.6)

and similarly for the expressions for a and h

$$a \simeq \frac{1}{z} \int_0^\infty dc \, c \, \sqrt{\pi} \frac{e^{\beta A(c)}}{\sqrt{\beta q} c^{1/4}} \simeq c^*, \qquad (C.7)$$

$$h \simeq \frac{1}{z} \int_0^\infty dc \, (c^2 - 2q \, \sqrt{c}) \, \sqrt{\pi} \frac{e^{\beta A(c)}}{\sqrt{\beta q} c^{1/4}}$$

$$\simeq c^{*2} - 2 \, \sqrt{c^*} q \simeq a^2 - 2a. \tag{C.8}$$

Analogously, we find $h_{nl} \simeq a^2$ and $h_{int} \simeq -2a$.

If now we substitute (C.6) and (C.7) in Eq. (C.5), we obtain

$$c^* = a = \frac{\mu + 1}{2},$$
 (C.9)

that is, a relation between a and the chemical potential μ for the MF model.

For the complete DNLS model, using the saddlepoint method we obtain a different relation between aand μ in the low-temperature limit

$$\mu_{DNIS}^{(T=0)} = 2(a-1)$$
 (C.10)

and if we replace a with Eq. (C.9) we obtain a relationship between the chemical potentials in the two models

$$\mu_{MF}^{(T=0)} = \mu_{DNLS}^{(T=0)} + 1. \tag{C.11} \label{eq:condition}$$

Appendix D. The ratio of energy differences R

If we combine Eqs. (B.14-B.17) retaining all terms up to the order w, we find

$$\Delta h_{nl} \equiv h_c - h_{nl} = \frac{4w}{m^2} \tag{D.1}$$

$$\Delta h \equiv h_c - h = \frac{4w}{m^2} + \frac{\pi w}{2}, \tag{D.2}$$

so that

$$R \equiv \frac{\Delta h_{nl}}{\Delta h} = \frac{4}{4 + \pi m^2/2} \tag{D.3}$$

which tends to $8a^2/\pi$ for small a and to 1 for large a.

References

- P. G. Kevrekidis, The discrete nonlinear Schrödinger equation: mathematical analysis, numerical computations and physical perspectives, Vol. 232, Springer Science & Business Media, 2009.
- [2] T. Mithun, Y. Kati, C. Danieli, S. Flach, Weakly nonergodic dynamics in the gross-pitaevskii lattice, Physical Review Letters 120 (18) (2018) 184101.
- [3] M. Giachello, S. Iubini, R. Livi, G. Gradenigo, Localization and "classical entanglement" in the discrete non-linear schr\" odinger equation, arXiv preprint arXiv:2503.14364 (2025).
- [4] M. Baldovin, S. Iubini, R. Livi, A. Vulpiani, Statistical mechanics of systems with negative temperature, Physics Reports 923 (2021) 1–50.
- [5] G. Tsironis, The discrete nonlinear schrödinger equation: From biomolecules to nonlinear optics to bose-einstein condensates, in: Artificial Intelligence and Complex Dynamical Systems, Springer, 2025, pp. 97–120.
- [6] S. Flach, C. R. Willis, Discrete breathers, Physics Reports 295 (5) (1998) 181–264.
- [7] S. Iubini, R. Franzosi, R. Livi, G.-L. Oppo, A. Politi, Discrete breathers and negativetemperature states, New Journal of Physics 15 (2) (2013) 023032.
- [8] B. Rumpf, Stable and metastable states and the formation and destruction of breathers in the discrete nonlinear schrödinger equation, Physica D: Nonlinear Phenomena 238 (20) (2009) 2067– 2077.
- [9] M. Ebrahimi, B. Drossel, W. Just, Dynamics of localised states in the stochastic discrete nonlinear schrödinger equation, Physica D: Nonlinear Phenomena 482 (2025) 134905.
- [10] S. Iubini, L. Chirondojan, G.-L. Oppo, A. Politi, P. Politi, Dynamical freezing of relaxation to equilibrium, Physical Review Letters 122 (8) (2019) 084102.

- [11] A. Politi, P. Politi, S. Iubini, Frozen dynamics of a breather induced by an adiabatic invariant, Journal of Statistical Mechanics: Theory and Experiment 2022 (4) (2022) 043206.
- [12] S. Machlup, Negative temperatures and negative dissipation, American Journal of Physics 43 (11) (1975) 991–995.
- [13] S. Iubini, A. Politi, P. Politi, Coarsening dynamics in a simplified dnls model, Journal of Statistical Physics 154 (4) (2014) 1057–1073.
- [14] G. Gotti, S. Iubini, P. Politi, Finite-size localization scenarios in condensation transitions, Physical Review E 103 (5) (2021) 052133.
- [15] M. Giusfredi, S. Iubini, P. Politi, Localization in boundary-driven lattice models, Journal of Statistical Physics 191 (10) (2024) 119.
- [16] M. Giusfredi, S. Iubini, A. Politi, P. Politi, Infinite-temperature thermostats by energy localization in a nonequilibrium setup, Journal of Statistical Mechanics: Theory and Experiment 2025 (5) (2025) 053203.
- [17] G. Gradenigo, S. Iubini, R. Livi, S. N. Majumdar, Localization transition in the discrete nonlinear schrödinger equation: ensembles inequivalence and negative temperatures, Journal of Statistical Mechanics: Theory and Experiment 2021 (2) (2021) 023201.
- [18] G. Gradenigo, S. Iubini, R. Livi, S. N. Majumdar, Condensation transition and ensemble inequivalence in the discrete nonlinear schrödinger equation, The European Physical Journal E 44 (3) (2021) 29, 1–6.
- [19] M. R. Evans, T. Hanney, Nonequilibrium statistical mechanics of the zero-range process and related models, Journal of Physics A: Mathematical and General 38 (19) (2005) R195.
- [20] S. Iubini, A. Politi, Effective grand canonical description of condensation in negative-temperature regimes, Physical Review Letters 134 (2025) 097102.
- [21] J. Szavits-Nossan, M. R. Evans, S. N. Majumdar, Constraint-driven condensation in large fluctuations of linear statistics, Physical Review Letters 112 (2) (2014) 020602.

- [22] G. Gotti, S. Iubini, P. Politi, Condensation induced by coupled transport processes, Physical Review E 106 (5) (2022) 054158.
- [23] K. Ø. Rasmussen, T. Cretegny, P. G. Kevrekidis, N. Grønbech-Jensen, Statistical mechanics of a discrete nonlinear system, Physical Review Letters 84 (17) (2000) 3740.
- [24] S. Iubini, S. Lepri, A. Politi, Nonequilibrium discrete nonlinear schrödinger equation, Physical Review E 86 (1) (2012) 011108.
- [25] G. E. Andrews, R. Askey, R. Roy, Special Functions, Encyclopedia of Mathematics and its Applications, Cambridge University Press, 1999.